Oxidative potential and water-soluble heavy metals of size-segregated airborne particles in haze and non-haze episodes: Impact of the “Comprehensive Action Plan” in China

Xiaolei Feng[1], Longyi Shao[1]*, Tim Jones[2], Yaowei Li[1], Yaxin Cao[1], Mengyuan Zhang[1], Shuoyi Ge[1], Chengxue Yang[3], Jing Lu[1], Kelly BéruBé[4]

[1] State Key Laboratory of Coal Resources and Safe Mining, and College of Geoscience and Surveying Engineering, China University of Mining and Technology (Beijing), Beijing 100083, China

[2] School of Earth and Environmental Sciences, Cardiff University, Park Place, Cardiff, CF10 3AT

[3]Institute of Earth Sciences, China University of Geosciences (Beijing), Beijing 100083, China

[4] School of Biosciences, Cardiff University, Museum Avenue, Cardiff, CF10 3AX, Wales, UK.

Highlights:

1. The highest level of particle-induced DNA damage decreased after the enactment of the CAP
2. The DNA damage was concentrated in the 'fine' particle size range (0.43-1.1μm) following the CAP
3. The DNA damage was predominantly caused by the heavy metals Pb, Cr, Cd, and Zn following the CAP
4. The heavy metals Pb, Cr, Cd, and Zn were concentrated in particles smaller than 2μm

Abstract

Air pollution is a major environmental health challenge in megacities, and as such a Comprehensive Action Plan (CAP) was issued in 2017 for Beijing, the capital city of China. Here we investigated the size-segregated airborne particles collected after the implementation of the CAP, intending to understand the change of oxidative potential and water-soluble heavy metal (WSHM) levels in 'haze' and 'non-haze' days. The DNA damage and the levels of WSHM were analyzed by Plasmid Scission Assay (PSA) and High-Resolution Inductively Coupled Plasma Mass Spectrometry (HR-ICP-MS) techniques. The PM mass concentration was higher in the fine particle size (0.43-2.1 μm) during haze days, except for the samples affected by mineral dust. The particle-induced DNA damage caused by fine sized particles (0.43-2.1 μm) exceeded that caused by the coarse sized particles (4.7-10 μm). The DNA damage from haze day particles significantly exceeded those collected on non-haze days. Prior to the instigation of the CAP, the highest value of DNA damage decreased, and DNA damage was seen in the finer size (0.43-1.1μm). The Pearson correlation coefficient between the concentrations of water-soluble Pb, Cr, Cd and Zn were positively correlated with DNA damage, suggesting that these WSHM had significant oxidative potential. The mass concentrations of water-soluble trace elements (WSTE) and individual heavy metals were enriched in the finer particles between 0.43 μm to 1.1 μm, implying that smaller sized particles posed higher health risks. In contrast, the significant reduction in the mass concentration of water-soluble Cd and Zn, and the decrease of the maximum and average values of DNA damage after the CAP, demonstrated its effectiveness in restricting coal-burning emissions. These results have demonstrated that the Beijing CAP policy has been successful in reducing the toxicity of 'respirable' ambient particles.

Keywords: health risk, respirable particles, Plasmid Scission Assay, size-segregated particulate matter, The Comprehensive Action Plan, water-soluble heavy metals

1. Introduction

As the capital of China and one of the World's major megacity, Beijing suffers from life-threating air pollution, which has been a monumental environmental challenge over the past two decades (Fu and Chen, 2017; Li et al., 2020b; Xing et al., 2020). To reduce the air pollution in Beijing, the "Air Pollution Prevention and Control Action Plan" (the Clean Air Action Plan) and the "Action Plan for Comprehensive Control of Atmospheric Pollution in Autumn and Winter of Beijing-Tianjin-Hebei region in 2017–2018" (the Comprehensive Action Plan, abbreviated as "CAP") were carried out (Li et al., 2020a; Liu et al., 2019; MEP, 2017; The State Council of China, 2013; Zhong et al., 2019). The air quality improvement after the implementation of the two action plans, when demonstrated by the annual mean concentration of $PM_{2.5}$ (airborne particulate matter with an aerodynamic diameter less than 2.5μm), revealed a reduction in the 'fine-sized' particle fraction (Beijing Ecology and Environment Statement, 2019). The particulate matter emissions from industry and coal combustion decreased after the implementation of the two action plans (Barrington-Leigh et al., 2019; Geng et al., 2019; Wang et al., 2020). In addition, the decreasing 'risk of death' brought on by reducing the levels of air pollution was a positive signal of improving air quality (Bi et al., 2019; Maji et al., 2020; Zhou et al., 2021). However, there are still annual incidences in Beijing when the air quality reaches unhealthy levels (Li et al., 2020a), e.g., when $PM_{2.5}$ values significantly exceeded the II Grade standard of the National Ambient Air Quality Standards (GB3095–2012) (MEP, 2012). These high values may be caused by regional transport, e.g., when $PM_{2.5}$ values changed from 4.40 $\mu g/m^3$ to 855.10 $\mu g/m^3$ (Wang et al., 2019; Zheng et al., 2015a). The regional transport of air masses and local emissions both affect air quality and may have an influence on PM components. A study on the mass concentration of trace elements in the rural mountainous site of Xinglong, a typical background site of northern China, determined that long-range transport caused an increase in trace elements (Pan et al., 2013).

Airborne particles, as important atmospheric pollutants, have a significant influence on morbidity and mortality (Apte et al., 2018; Silva et al., 2021; Ren et al.,

2021; Xue et al., 2019). Epidemiological investigations have shown that airborne PM has adverse health effects in Beijing (Chen et al., 2020; Huang et al., 2018a; Sheehan et al., 2016). Exposure to high levels of $PM_{2.5}$ can lead to premature death (Liu et al., 2016; Maji et al., 2018; Zheng et al., 2015b), cardiovascular diseases (Lin et al., 2019; Ma et al., 2019), chronic obstructive pulmonary disease (Guo et al., 2020; Song et al., 2017), respiratory disease (Crabbe, 2012; Han et al., 2020) and lung cancer (Chen et al., 2016; Cohen et al., 2017; Pirozzi et al, 2018). However, the toxic mechanisms underlying the adverse health effects following inhalation exposure to particles remains unclear. An extensively accepted hypothesis is that PM-induced oxidative stress causes toxic effects (Shao et al., 2017). The studies of physicochemical characteristics and toxicology of particles have revealed that the heavy metals in the particulate matter can cause oxidative damage in humans (Conibear et al., 2018; Gao and Ji, 2018; Rohra et al., 2018; Silva et al., 2021; Wu et al., 2021). Moreover, the heavy metals bound to particulate matter differ with particle size and mass concentration (Lyu et al., 2017). Therefore, it is important to study the components of size-segregated airborne particles, especially heavy metals, to understand the particle-induced damage and resulting human health risk.

Many methods are being employed to assess the oxidative potential of atmospheric particles, such as the Ames test (Du et al., 2019), dithiothreitol (DTT) -driven assay (Carville et al., 2013), hemolysis assay (Zhang et al., 2019; Mesdaghinia et al., 2019), comet assay (Bahadori et al., 2018), and plasmid scission assay (PSA) (Shao et al., 2017). The PSA is an *in vitro* method to evaluate PM oxidative capacity and then semi-quantify particulate bioreactivity (Lawson et al., 2020; Bandowe et al., 2021; Niu et al., 2021). PSA has been used due to the simplicity, rapid high-throughput, high sensitivity, and reproducibility of the assay (Feng et al., 2020; Shao et al., 2006, 2013, 2016; Sun et al., 2014).

In this study, ambient PM were collected in 2018 after the instigation of the CAP program in Beijing, and the oxidative capacities and heavy metal compositions of size-segregated particles were determined. The relationships between the levels of WSHM

and DNA damage were analyzed. Finally, a comparison between the WSHM compositions of size-segregated haze particles, both before and after the CAP, was made to elucidate the CAP's effect on harmful elements in airborne particles.

2. Sampling and Methods

2.1 Sampling

The sampling site was situated at the China University of Mining and Technology (Beijing) in Haidian District, Beijing. The sampling site was on the North Fourth Ring Road 1km to the south, with Xueyuan Road (one of the main roads in Beijing) 100 m to the east. The sampler was installed outside on the top of the fourth floor of the Comprehensive Building, approximately 18m above the ground. This collection site was part of a typical campus and residential area in Beijing, with no large heavy industrial pollution sources in the immediate area.

An eight-stage Anderson cascade impact sampler (TE-20-800 TISCH, Germany) was used, with a collection height of 1.5 m higher than the floor on which it was located. The sampling flow rate utilized was 28.3 L/min. The sampler effectively separated the PM into 8 equivalent cut-off diameters (μm): 0.43-0.65, 0.65-1.1, 1.1-2.1, 2.1-3.3, 3.3-4.7, 4.7-5.8, 5.8-9.0, 9.0-10. Quartz fiber filters (80 mm diameter, Millipore, China) were used to collect the different sized particles. The sampling period was conducted from November 30th to December 4th in 2018, and the sampling time was 23.5 hours from 9:00 to 8:30 the next day. The meteorological data were obtained from a portable meteorological instrument (Kestrel 5500 Weather LiNK, USA: Supplementary Table S1 during sampling period). The quartz fiber filters were heated at 450℃ for 4 hours by a muffle furnace (ZK-6XY-1400, Beijing ZHONGKEBEIYIKEJI, China), and placed in a constant temperature and humidity chamber (Hitachi, Japan; temperature: 20℃±5℃, relative humidity: 45% ± 5%) for 48 hours before sampling and weighing.

The mass concentrations of size-segregated particles were obtained using the gravimetric method. The fiber filters were weighed using an electronic balance (Sartorius CP225D, Switzerland) with an accuracy of 0.01 mg. The formula calculating

147 the mass concentration, as defined by Feng et al. (2020), was employed.
148
149 **2.2 Plasmid scission assay**
150 The PSA is an *in vitro* method to determine the oxidative potential. The principle
151 of the assay is that free radicals induced by heavy metals occurring on the surfaces of
152 the particles can damage the supercoiled plasmid DNA. The initial oxidative damage
153 causes the supercoiled DNA to relax, and the maximum extent of damage results in
154 linearization. The relative electrophoretic mobility of supercoiled, relaxed, and
155 linearized DNA in the gel analysis system (Synoptics Ltd., Cambridge, UK) was used
156 to calculate the percentages of the three forms of plasmid DNA. The total percentages
157 of the relaxed and linearized DNA were taken as the level of oxidative damage.
158 Ultra-pure water (conductivity 18.2 MΩ, Millipore, China) was used as the blank
159 sample for each group of pollution samples. The value of the blank oxidative damage
160 was subtracted from the sample DNA damage. Four parallel samples were run in each
161 group. The details on the methodology were as follows:
162 (1) Preparation of water-soluble sample: the filters and blank filter were cut into 5mm
163 squares and put into a 15 ml centrifuge tube (Corning, USA). A measured amount
164 of ultra-pure water was added to the centrifuge tube to make the particle dosage of
165 100 μg/ml. Each sample solution was mixed for 20 hours using a platform shaker
166 (VORTEX-GENIE2, Scientific Industries, USA). The solution was transferred to a
167 1.5 ml centrifuge tube by pipette (Eppendorf, Germany). A Kendro centrifuge (D-
168 37520 Osterode, Germany) centrifuged the solution for 80 s and the supernatant
169 was extracted.
170 (2) DNA sample and gel preparation: 82 μl of the sample supernatant and 4 μl of the
171 plasmid X174-RF DNA (Promega, USA) was added to a 1.5 ml centrifuge tube.
172 This was oscillated horizontally for 6 hours to ensure a good mixing (HX-3000,
173 YOUNING, China). Agarose (molecular biology grade; Sigma-Aldrich, China) was
174 dissolved in 100 *X* Tris/Borate/EDTA (TBE) buffer solution (Thermo Scientific,
175 China) and the solution was heated to transparency. Ten millilitres of ethidium

bromide (EB; Sigma-Aldrich, China) was added to the agarose solution when cooled to 78℃, and this forms a gel on the electrophoresis plate (DYCP34C; LIUYI, China).

(3) Fourteen microliters of bromophenol blue stain (Sigma- Aldrich, China) was added to the mixture of the sample supernatant, and DNA was injected into the solidified gel wells. Each gel well was injected with 20 μl of the final solution. The electrophoresis apparatus (DYY-6C, LIUYI, China) was operated at 30 volts for 16 hours at room temperature.

(4) Analysis of DNA damage: the variation of DNA morphologies was observed and quantified by the UV gel imaging system (ChemiDoc, Bio-red, China) and the Syngene Genetools software (version 4.0; Syngene, USA).

2.3 High-Resolution Inductively Coupled Plasma Mass Spectrometry

Each PM sample was immersed in a measured amount of ultra-pure water to make the soluble concentration of 100 μg/ml and was shaken for 20 hours. The water-soluble sample was obtained from the centrifuged supernatant (D-37520 Osterode, Germany), after spinning at 13000 rpm for 80 minutes. The WSTE compositions of the samples were analyzed in a High-Resolution Inductively Coupled Plasma Mass Spectrometer (HR-ICP-MS; ThermoFisher; Element XR). Forty-three WSTE were examined. Seven typical heavy metals within the detection limit were analyzed, namely, Zn, Cu, Pb, Ni, Cd, Cr, and Co (values shown in Table S2). The mass concentration of the WSHM elements (ng/m^3) was calculated using the formula:

$$C = \frac{c \times Vt}{Vs}$$

Where: C represents the mass concentration of the water-soluble element (ng/m^3); c represents the trace element level in the water-soluble sample (μg/ml); Vt represents the total solution volume (ml), Vs represents standard sample volume (m^3)

3. Results

3.1 The mass concentration of $PM_{2.5}$ during the haze episode

In this study, the specific $PM_{2.5}$, SO_2, NO_2, and O_3 mass concentration data were obtained from data published by the Wanliu State-Control Air Monitoring Station (https://github.com/tuanvvu) during the sampling period (Fig.S1.). The $PM_{2.5}$ accumulation stage began at 13:00 on November 30th. At 02:00 on December 3rd, the $PM_{2.5}$ mass concentration began to decrease, from 154 μg/m^3 to 121 μg/m^3 at 03:00. At 05:00 on December 3rd, the $PM_{2.5}$ mass concentration significantly decreased, from 112 μg/m^3 at 04:00 to 93 μg/m^3 (Fig.S1.). Based on the data, sample A represented moderate pollution, samples B and C indicated heavy pollution, and sample D denoted a non-haze day.

3.2 Mass concentration of size-segregated particles in haze and non-haze days

The mass concentrations of size-segregated particles in haze days were higher than those on non-haze days, although the size distributions appeared similar (Fig.2). The levels were also higher in heavy pollution days of samples B and C when compared to those in the moderate pollution of sample A.

The mass concentrations of different sized particles were different in haze days. For the moderate pollution of sample A and heavy pollution of sample B, the mass concentration of size-segregated particles in the fine size scale of 0.43-2.1 μm was higher than that in the coarser sized PM (i.e., 4.7-10 μm). The level of sample C increased in the large particle size fraction of 4.7-10 μm, which is believed to be due to mineral dust that would be expected in the larger size fractions of 5.8-10 μm. The PM mass concentration increased with increased particle size in the non-haze day of sample D.

3.3 Oxidative potential of water-soluble components in size-segregated airborne particles

Previous studies have demonstrated that the DNA damage caused by the whole sample was like that caused by water-soluble components, indicating that the DNA damage was mainly induced by the water-soluble components in particles (Lv et al.,

2006; Shao et al., 2006, 2007, 2017; Song et al., 2015). It is confirmed in many prior studies that the DNA damage of each sample increases with the increased particle dosage (Shao et al., 2006, 2007, 2017; Xiao et al., 2014), and for the expediency of comparison between different samples, we took the DNA damage percentage at the particle dosage of 100 μg/ml (Table 1). The particulate mass within the 0.43-1.1 μm size zone in the non-haze day sample was too low to perform the PSA at the selected comparative particle dosage of 100 μg/ml.

When comparing the DNA damage induced by the water-soluble fractions of the size-segregated particles, the DNA damage in the 0.43-2.1 μm size exceeded that in the 4.7-10 μm size fraction. In addition, the DNA damage in the smaller size range of 0.43-1.1 μm was significantly higher than that in the 1.1-2.1 μm range. In haze days, the DNA damage decreased first in the PM fraction ranging from 0.43 μm to 2.1 μm (aerodynamic diameter) and then increased in the size range of 5.8 μm to 10 μm with increased particle size. In the 0.43-1.1μm size limit, the DNA damage of sample A was higher than that of samples B and C. In the 1.1-2.1μm size span, the DNA damage of sample B was higher than that of samples A and C. DNA damages induced by samples B and C were higher than that induced by sample A in 2.1-10 size limit. In conclusion, the DNA damage was highest in the smaller sized PM, i.e., 0.43 μm to 1.1 μm (aerodynamic diameter).

The DNA damage caused by size-segregated particles in haze days was higher than that on the non-haze days. The variability of DNA damage was not significant with increased particle size on non-haze days.

3.4 The mass concentration of WSHM in size-segregated particles

The mass concentrations of the total WSTE and individual WSHM could present a health risk above certain levels of PM exposure (Fig.3). The mass concentration of the total WSTE, which represented the sum of the contents of the total 43 trace elements in size-segregated particles detected, is shown in Fig.3. The mass concentration of total WSTE in haze days was higher than that on the non-haze days. Over the course of the

haze days, the mass concentration of total WSTE had a normal distribution over the particle size range, with the peak value at 1.1-2.1 μm. In the 0.43-1.1 μm size range, the mass concentration of total WSTE of sample A was higher than that of sample B and sample C, which corresponded to the level of DNA damage (Table 1). In the 1.1-2.1 μm size range, the mass concentration of total WSTE within sample B was higher than that of samples A and C, again corresponding to the level of the DNA damage (Table 1). These results indicated that the particles below 2.1 μm would present a higher health risk than those above this size.

The mass concentrations of Pb and Cr were noticeably higher during haze days when compared to non-haze days. There was no significant variation and very low levels with increased particle size on the non-haze days. However, the mass concentration of Cr decreased with the increased particle sizes on the non-haze day (Fig.3). During haze days, the mass-size distribution of Pb and Cr was highest in the fine PM (i.e., 0.43-2.1 μm). For Pb and Cr, the highest value of mass concentration in the moderate pollution of sample A appeared in the 0.65-1.1 μm fraction, whereas in the heavy pollution of samples B and C the highest values appeared in the PM limited between 1.1 μm to 2.1 μm (aerodynamic diameter). Interestingly, the mass concentration in the moderate pollution of sample A was significantly higher than that in the heavy pollution of samples B and C.

The mass concentrations of Cd and Zn in both the haze and the non-haze days demonstrated a remarkable similarity. The haze day samples were enriched in both metals in the small size range (i.e., 0.43-2.1 μm; Fig.3). The mass-size distribution of Cd and Zn in the heavy pollution of samples B and C was most significant in the 1.1 μm to 2.1 μm size range (aerodynamic diameter). For the moderate pollution of sample A, the mass-size distribution of Cd was greatest in the 0.56 μm to 1.1 μm range, and that of Zn was highest in the 1.1 μm to 2.1 μm PM distribution. The mass concentrations of Cd and Zn revealed no significant variation with increased particle size on the non-haze days.

For Co, Ni, and Cu, the mass-size distribution was highest in PM larger than 1.1

μm (aerodynamic diameter) in haze days (Fig.3). The mass of Cu was concentrated in particles within the respirable size range (i.e., 1.1-3.3 μm), and that of Co enriched in PM capable of 'thoracic' deposition (2.1 to 5.8 μm) within the human respiratory system. The mass of Ni from the moderate pollution of sample A and heavy pollution of sample C was concentrated in the respirable range (1.1 to 2.1 μm), and from the heavy pollution of sample B, concentrated within the inhalable fraction (e.g., 3.3-5.8 μm). The mass concentrations of Co, Ni, and Cu showed no significant variation with increased particle size on the non-haze days.

4. Discussion

4.1 Correlation between concentrations of WSTE and particle-induced DNA damage

The levels of the typical WSHM above the detection limits were obtained by HR-ICP-MS. The connection between the concentrations of the typical WSHM and the corresponding DNA damage at the particle dosage of 100 μg/ml were analyzed (Table 2). According to the correlation analysis, the correlation coefficient was higher than the critical value of 0.449 at the 0.01 significance level with a sample number N=30, indicating that the types of WSTE and DNA damage were related. The correlation coefficients of four heavy metals were significantly higher than other elements, namely Cr, Zn, Cd, and Pb (Table 2).

The relationship between the DNA damage and the levels of total WSTE was markedly positive, with a correlation coefficient of 0.558, indicating that the total WSTE had a significant role in particle-induced oxidative potential. The individual heavy metals Pb, Cr, Cd and Zn also showed a markedly positive correlation with DNA damage, and their correlation coefficients were higher than the critical value of 0.449. The correlation coefficient between DNA damage and Pb was the highest, with a coefficient of 0.595. The correlation coefficients of water-soluble Cu, Ni, and Co were 0.316, 0.303, and 0.114, respectively, and all of them were lower than the critical value of 0.449.

4.2 Comparison between the DNA damage induced by the water-soluble fractions of size-segregated haze particles before and after the CAP

To improve the air quality of Beijing, the government implemented a series of control measures in 2017, called the "Comprehensive Action Plan" (abbreviated to "CAP"). The data for the particle-induced DNA damage before the CAP originated from Sun et al. (2014), who investigated the airborne particles collected in 2010. Particulate matter collected over the described size ranges indicated a different pattern of oxidative capacity before and after the implementation of the CAP (Sun et al, 2014). Fig.4 shows the variations of the particle-induced DNA damage over the particle size range in haze days before and after the CAP. Since the PM ranged from 0.056 μm to 0.32 μm in 2010 were much smaller than those in 2018 (i.e., 0.43 to 0.65 μm), the size limit of 0.056 μm to 0.32 μm could not be used for comparison. The size range of 0.43-10 μm in 2018 was closer to that reported in 2010 (i.e., 0.32-10 μm), and thus the DNA damage caused by these two particle fractions were utilized for comparison. It was noted that although the sizes were marginally different, the overall trends were self-evident.

Overall, the level of DNA damage in 2018 was reduced in comparison to the levels in 2010. The DNA damage was highest in the 0.43-1.1 μm size range after the CAP policy was initiated, whereas the DNA damage was highest in the 1.0-3.2 μm size range before the CAP, implying that after the CAP, the greater oxidative potential moved to the finer particle size, especially those smaller than 2.0 μm (Fig.4). Previous studies have shown that the heavy metals were generally enriched in smaller particles which is a globally observed phenomenon (Lyu et al., 2017; Tan et al., 2016; Sun et al., 2014; Song and Gao, 2011). In addition, it was reported that the secondary particles have smaller particle sizes and carry more trace elements (Gao et al., 2015; Dong et al., 2020).

The highest value of the average DNA damage in 2018 decreased when compared with that in 2010 (Fig.5). It was noted that the DNA damage induced by the large particle size range (i.e., > 5.0 μm) slightly increased in 2018 in comparison with that in

2010, which needs to be investigated further in the future, although this small variation might be related to more aged secondary particles after the CAP (Shao et al., 2021). Fig.5 displayed the significant reduction in DNA damage by fine particles (i.e., 1 μm to 3 μm aerodynamic diameter), however the particle-induced DNA damage after the CAP exhibited an insignificant decreasing trend with the increase of the particle size. This possibly suggested a less obvious trend, whereby the greater oxidative potential has translocated into the finer PM fraction, especially in particles smaller than 2.0 μm.

4.3 Comparison between the WSHM compositions of size-segregated haze particles before and after the CAP

Heavy metals are believed to influence the radical generating capacity and then effect the variation of the oxidative damage (Tian et al., 2021; Shao et al., 2017). To study the causes of oxidative damage before and after the CAP, the mass concentration of WSHM from different sized particles during haze days was compared and analyzed. Fig.6 demonstrated that the mass concentrations of WSHM Pb, Cr, Cd, and Zn in size-segregated particles, which were positively correlated with DNA damage before and after the CAP, were enriched in the small particle size range for both before and after the CAP. Despite this, the highest values before the CAP were observed in the less than 1.4 μm size range, and the highest values after the CAP were identified in the less than 1.6 μm size range. This indicated that after the CAP, the mass concentration of WSHM was still enriched in the fine size range, although the particle size range has widened to less than 2.0 μm, which may be related to the more complicated secondary formations of particles (Shao et al., 2021).

The Pb and Cr masses were concentrated in the small size range of 0.43-2.1μm after the CAP in this study, and this was like the studies on the mass-size distribution of heavy elements in heavy pollution episodes in Beijing in winter before the CAP, which found that the Pb and Cr were mainly concentrated in the 1-2 μm size range (Li et al., 2012; Tan et al., 2016). The highest mass concentrations of Cd and Zn appeared in the 0.56-1.0μm size range in the Beijing atmosphere after the Olympic games (Li et

al., 2012). These facts illustrated that Pb, Cr, Cd, and Zn were enriched in the fine size range.

For the individual elements, the mass concentration of water-soluble Pb and Cr in size-segregated particles was significantly increased, whereas that of Cd and Zn was decreased over the particle size range after the CAP (Fig.6). In the 1-3 μm size range, the mass concentrations of Cd and Zn in 2018 were lower than that in 2010, corresponding to the variation of the average DNA damage as shown in Fig.5.

The source apportionment of Zn and Cd in airborne PM found that coal-burning emissions was the major contributor (Li et al., 2017; Liu et al., 2021). The major control measures of the Clean Air Action Plan and CAP include coal-fired emissions, industrial emissions, vehicle emissions, dust emissions, and other measures. These measures greatly controlled coal combustion (Li et al., 2020; Xu and Zhang, 2020). The mass concentration of Zn, where Cd slightly decreased after the CAP, suggested that the reduction of coal-burning emissions played an important role in alleviating Beijing's air pollution.

Source apportionment in the Beijing atmosphere showed that traffic-related emission was the dominant source of Cr (Huang et al., 2018b). According to the data of the Beijing Municipal Bureau of Statistics, car ownership in Beijing increased from 4.81 million in 2010 to 6.08 million in 2018 (http://jtgl.beijing.gov.cn), which has resulted in the mass concentration of Cr increasing after the CAP. Therefore, vehicle emission controls should be increased.

Since 2003, Pb has been prohibited in gasoline, whereas the mass concentration of Pb increased after the CAP. Therefore, this suggests that Pb may come from other sources, such as regional transport (Lv et al., 2021; Wang et al., 2017; Zhang et al., 2019) and yellow traffic paint (O'Shea et al., 2021), although this inference needs to be further validated by more detailed studies.

5. Conclusions

(1) The DNA damage induced by water-soluble components at the particle dosage

of 100μg/ml in the smaller size ranges of 0.43-1.1μm was higher than that in the large size ranges of 4.7-10μm, and the DNA damage in the haze days was higher than that in the non-haze days.

(2) After the CAP, the DNA damage induced by the water-soluble components at the particle dosage of 100μg/ml was slightly higher in the size range less than 1μm, implying that the oxidative potential of finer particles increased after the CAP. Although the DNA damage was slightly higher in the size range less than 0.6μm after the CAP, the DNA damage significantly decreased in the size ranges 1-3 μm after the CAP.

(3) Before and after the CAP, the positive correlation between the DNA damage and the water-soluble Pb, Zn, Cd, and Cr showed that these water-soluble heavy metals were most likely responsible for the oxidative potentials.

(4) The mass concentration of Zn, Cd slightly decreasing after the CAP, suggested that the reduction of coal-burning emissions played an important role in alleviating Beijing's air pollution. However, the mass concentration of Pb and Cr increasing after the CAP implied that Pb and Cr were affected by other factors, such as regional transport and traffic-related sources, although this inference needs to be further validated by more detailed studies.

Acknowledgments

This study is supported by the National Natural Science Foundation of China (Grant No. 420750441), the Fundamental Research Funds for the Central Universities. The authors are indebted to Bob Finkelman for his constructive discussion and comments.

References

Apte, J.S., Brauer, M., Cohen, A.J., Ezzati, M., Pope, C.A. III., 2018. Ambient $PM_{2.5}$ reduces global and regional life expectancy. *Environmental Science & Technology Letters 5*, 546-551. 10.1021/acs.estlett.8b00360.

Bahadori, F., Kocyigit, A., Onyuksel, H., Dag, A., Topcu, G., 2018. Cytotoxic, apoptotic and genotoxic effects of lipid-based and polymeric nano micelles, an in vitro evaluation. Toxics 6 (1), e0007. https://doi.org/10.3390/toxics6010007.

Bahrami, F., Esfarjani, F., Marandi, S.M., 2013. Effects of intermittent exercise in polluted and clean air on hemolysis of red blood cells in Endurance Runners. J. *Isfahan Med. School 30 (212)*, 1845–1855.

Bandowe, Benjamin A.Musa, Lui, K.H., Jones, T., BeruBe, K., Adams, R., Niu, X.Y., Wei, C., Cao, J.J., Lee, S.C., Chuang, H.C., Ho, K.F., 2021. The chemical composition and toxicological effects of fine particulate matter ($PM_{2.5}$) emitted from different cooking styles. *Environmental Pollution 288*, 117754. 10.1016/j.envpol.2021.117754.

Barrington-Leigh, C., Baumgartner, J., Carter, E., Robinson, B. E., Tao, S., Zhang, Y. 2019. An evaluation of air quality, home heating and well-being under Beijing's programme to eliminate household coal use. *Nature Energy 4*, 416-423. 10.1038/s41560-019-0386-2.

Beijing Ecology and Environment Statement, 2019. Beijing municipal ecology and environment bureau. http://sthjj.beijing.gov.cn/bjhrb/index/xxgk69/sthjlyzwg/1718880/1718881/1718882/1791057/index.html. (Accessed 27 April 2020) (in Chinese).

Bi, W., Chen, K., Xiao, Z., Tang, M., Zheng, N., Yang, N., Gao, J., Li, Y., Kong, J., Xu, H., 2019. Health Benefit Assessment of China's National Action Plan on Air Pollution in the Beijing-Tianjin-Hebei Area. *Aerosol and Air Quality Research 19*, 383-389. 10.4209/aaqr.2018.08.0297.

Carville, G.B., Christoph, K., Christoph, R., Hélène, T., Katja, K., Matthias, W., Johannes, O., 2013. Determination of the warfarin inhibition constant Ki for vitamin K 2,3-epoxide reductase complex subunit-1 (VKORC1) using an in vitro DTT-driven assay. *Biochim. Biophys. Acta 1830,* 4202–4210. 10.1016/j.bbagen.2013.04.018.

Chen, X., Zhang, L.W., Huang, J.J., Song, F.J., Zhang, L.P., Qian, Z.M., Trevathan, E., Mao, H.J., Han, B., Vaughn, M., Chen, K.X., Liu, Y.M., Chen, J., Zhao, B.X., Jiang, G.H., Gu, Q., Bai, Z.P., Dong, G.H., Tang, N.J., 2016. Long-term exposure to urban air pollution and lung cancer mortality: A 12-year cohort study in Northern China. *Science of the Total Environment 571*, 855-861. 10.1016/j.scitotenv.2016.07.064.

Chen, X., Qiu, B., Zou, Q.P., Qiu, T., Li, R.K., Truong, A., Qi, Y.M., Liu, T., Han, L.M., Liu, T.B., Chang, J.R., Sun, Q., Zhu, Y., Xu, D.Q., 2020. Source specific $PM_{2.5}$ associated with heart rate variability in the elderly with coronary heart disease: A community-based panel study. *Chemosphere 260*. 10.1016/j.chemosphere.2020.127399.

Cohen, A.J., Brauer, M., Burnett, R., Anderson, H.R., Frostad, J., Estep, K.,

Balakrishnan, K., Brunekreef, B., Dandona, L., Dandona, R., Feigin, V., Freedman, G., Hubbell, B., Jobling, A., Kan, H., Knibbs, L., Liu, Y., Martin, R., Morawska, L., Pope, C.A., III, Shin, H., Straif, K., Shaddick, G., Thomas, M., van Dingenen, R., van Donkelaar, A., Vos, T., Murray, C.J.L., Forouzanfar, M.H., 2017. Estimates and 25-year trends of the global burden of disease attributable to ambient air pollution: an analysis of data from the Global Burden of Diseases Study 2015. *Lancet 389*, 1907-1918. 10.1016/s0140-6736(17)30505-6.

Crabbe, H., 2012. Risk of respiratory and cardiovascular hospitalisation with exposure to bushfire particulates: new evidence from Darwin, Australia. *Environmental Geochemistry and Health 34*, 697-709. DOI: 10.1007/s10653-012-9489-4.

Dong, Z.S., Su, F.C., Zhang, Z.Y., Wang, S.B., 2020. Observation of chemical components of $PM_{2.5}$ and secondary inorganic aerosol formation during haze and sandy haze days in Zhengzhou, China. *Journal of Environmental Sciences 88,* 316-325. 10.1016/j.jes.2019.09.016.

Du, X.M., Gao, S.X., Hong, L.L., Zheng, X., Zhou, Q.Y.,Wu, J.H., 2019. Genotoxicity evaluation of titanium dioxide nanoparticles using the mouse lymphoma assay and the Ames test. *Mutat Res-Gen. Tox. En. 838,* 22–27. doi: 10.1016/j.mrgentox.2018.11.015.

Feng, X.L., Shao, L.Y., Xi, C.X., Jones, T.P., Zhang, D.Z., BeruBe, K.A., 2020. Particle-induced oxidative damage by indoor size-segregated particulate matter from coal-burning homes in the Xuanwei lung cancer epidemic area, Yunnan Province, China. *Chemosphere 256*, 127058. DOI: ARTN 127058 10.1016/j.chemosphere.2020.127058.

Fu, H.B., Chen, J.M., 2017. Formation, features and controlling strategies of severe haze-fog pollutions in China. *Science of the Total Environment 578*, 121-138. DOI: 10.1016/j.scitotenv.2016.10.201.

Gao, Y., Ji, H.B., 2018. Microscopic morphology and seasonal variation of health effect arising from heavy metals in $PM_{2.5}$ and PM_{10}: One-year measurement in a densely populated area of urban Beijing. *Atmospheric Research 212*, 213-226. DOI: 10.1016/j.atmosres.2018.04.027.

Gao, J.J., Tian, H.Z., Cheng, K., Lu, L., Zheng, M., Wang, S.X., Hao, J.M., Wang, K., Hua, S.B., Zhu, C.Y., Wang, Y., 2015. The variation of chemical characteristics of $PM_{2.5}$ and PM_{10} and formation causes during two haze pollution events in urban Beijing, China. *Atmospheric Environment 107*, 1-8. 10.1016/j.atmosenv.2015.02.022.

Geng, G., Xiao, Q., Zheng, Y., Tong, D., Zhang, Y., Zhang, X., Zhang, Q., He, K., Liu, Y., 2019. Impact of China's Air Pollution Prevention and Control Action Plan on $PM_{2.5}$ chemical composition over eastern China. *Science China-Earth Sciences 62*, 1872-1884. 10.1007/s11430-018-9353-x.

Guo, C.X., Sun, X.Y., Diao, W.Q., Shen, N., He, B., 2020. Correlation of clinical symptoms and sputum inflammatory markers with air pollutants in stable COPD patients in Beijing area. *International Journal of Chronic Obstructive Pulmonary Disease 15*, 1507-1517. 10.2147/copd.S254129.

Han, L., Sun, Z.B., He, J., Hao, Y., Tang, Q.L., Zhang, X.L., Zheng, C.J., Miao, S.G., 2020. Seasonal variation in health impacts associated with visibility in Beijing, China. *Science of the Total Environment 730*, ARTN 139149 10.1016/j.scitotenv.2020.139149.

Huang, J., Pan, X.C., Guo, X.B., Li, G.X., 2018a. Health impact of China's Air Pollution Prevention and Control Action Plan: an analysis of national air quality monitoring and mortality data. *The Lancet Planetary Health 2*, e313-e323. 10.1016/s2542-5196(18)30141-4.

Huang, R.J., Cheng, R., Jing, M., Yang, L., Li, Y.J., Chen, Q., Chen, Y., Yan, J., Lin, C.S., Wu, Y.F., Zhang, R.J., El Haddad, I., Prevot, A.S.H., O'Dowd, C.O., Cao, J.J., 2018b. Source-specific health risk analysis on particulate trace elements: coal combustion and traffic emission as major contributors in wintertime Beijing. *Environmental Science & Technology 52*, 10967-10974. 10.1021/acs.est.8b02091.

Lawson, M.J., Prytherch, Z.C., Jones, T.P., Adams, R.A., Berube, K.A., 2020. Iron-rich magnetic coal fly ash particles induce apoptosis in human bronchial cells. Applied Sciences 10 (23) , 8368. 10.3390/app10238368

Li, R., Li, J.L., Cui, L.L., Wu, Y., Fu, H.B., Chen, J.M., Chen, M.D., 2017. Atmospheric emissions of Cu and Zn from coal combustion in China: Spatio-temporal distribution, human health effects, and short-term prediction. *Environmental Pollution 229,* 724-734. 10.1016/j.envpol.2017.05.068.

Li, W.J., Shao, L.Y., Wang, W.H., Li, H., Wang, X.M., Li, Y.W., Li, W.J., Jones, T.P., Zhang, D.Z., 2020a. Air quality improvement in response to intensified control strategies in Beijing during 2013-2019. *Sci Total Environ 744*, 140776. 10.1016/j.scitotenv.2020.140776

Li, X.R., Wang, L.L., Wang, Y.S., Wen, T.X., Yang, Y.J., Zhao, Y.N., Wang, Y.F., 2012. Chemical composition and size distribution of airborne particulate matters in Beijing during the 2008 Olympics. *Atmospheric Environment 50*, 278-286. 10.1016/j.atmosenv.2011.12.021.

Li, Y.W., Shao, L.Y., Wang, W.H., Zhang, M.Y., Feng, X.L., Li, W.J., Zhang, D.Z., 2020b. Airborne fiber particles: types, size and concentration observed in Beijing. *Sci Total Environ 705*, 135967. 10.1016/j.scitotenv.2019.135967.

Lin, X., Liao, Y., Hao, Y.T., 2019. The burden of cardio-cerebrovascular disease and lung cancer attributable to $PM_{2.5}$ for 2009, Guangzhou: a retrospective population-based study. *International Journal of Environmental Health Research 29*, 582-592. 10.1080/09603123.2018.1557605

Liu, J., Han, Y.Q., Tang, X., Zhu, J., Zhu, T., 2016. Estimating adult mortality attributable to $PM_{2.5}$ exposure in China with assimilated $PM_{2.5}$ concentrations based on a ground monitoring network. *Science of the Total Environment 568*, 1253-1262. 10.1016/j.scitotenv.2016.05.165.

Liu, Y. Y., Xing, J., Wang, S. X., Fu, X., Zheng, H. T. 2018. Source-specific speciation profiles of $PM_{2.5}$ for heavy metals and their anthropogenic emissions in China. *Environmental Pollution 239*, 544-553. 10.1016/j.envpol.2018.04.047.

Liu, Z.R., Hu, B., Ji, D.S., Cheng, M.T., Gao, W.K., Shi, S.Z., Xie, Y.Z., Yang, S.H.,

Gao, M., Fu, H.B., Chen, J.M., Wang, Y.S., 2019. Characteristics of fine particle explosive growth events in Beijing, China: Seasonal variation, chemical evolution pattern and formation mechanism. *Science of the Total Environment 687*, 1073-1086. 10.1016/j.scitotenv.2019.06.068.

Liu, Z., Zhang, H., Zhang, Y., Liu, X., Ma, Z., Xue, L., Peng, X., Zhao, J., Gong, W., Peng, Q., Du, J., Wang, J., Tan, Y., He, L., Sun, Y., 2021. Characterization and sources of trace elements in PM_1 during autumn and winter in Qingdao, Northern China. *Sci Total Environ.* 10.1016/j.scitotenv.2021.151319151319.

Lv, S.L., Shao, L.Y., Wu, M.H., Jones, T.P., Merolla, L., Richard, R.J., 2006. Correlation between plasmid DNA damage induced by PM10 and trace metals in inhalable particulate matters in Beijing air. *Science in China Series D: Earth Sciences 49*, 1323-1331. 10.1007/s11430-006-2020-y.

Lv, L. L., Chen, Y. J., Han, Y., Cui, M., Wei, P., Zheng, M., Hu, J. N. 2021. High-time-resolution $PM_{2.5}$ source apportionment based on multi-model with organic tracers in Beijing during haze episodes. *Science of the Total Environment 772*, 144766. ARTN 144766 10.1016/j.scitotenv.2020.144766

Lyu, Y., Zhang, K., Chai, F.H., Cheng, T.T., Yang, Q., Zheng, Z.L., Li, X., 2017. Atmospheric size-resolved trace elements in a city affected by non-ferrous metal smelting: Indications of respiratory deposition and health risk. *Environ Pollut 224*, 559-571. 10.1016/j.envpol.2017.02.039.

Ma, Y.X., Yang, S.X., Yu, Z., Jiao, H.R., Zhang, Y.F., Ma, B.J., 2019. A study on the short-term impact of fine particulate matter pollution on the incidence of cardiovascular diseases in Beijing, China. *Atmospheric Environment 215*, 10.1016/j.atmosenv.2019.116889.

Maji, K.J., Dikshit, A.K., Arora, M., Deshpande, A., 2018. Estimating premature mortality attributable to $PM_{2.5}$ exposure and benefit of air pollution control policies in China for 2020. *Science of the Total Environment 612*, 683-693. 10.1016/j.scitotenv.2017.08.254.

Maji, K. J., Li, V. O. K., Lam, J. C. K., 2020. Effects of China's current Air Pollution Prevention and Control Action Plan on air pollution patterns, health risks and mortalities in Beijing 2014-2018. *Chemosphere 260*, 10.1016/j.chemosphere.2020.127572.

Mesdaghinia, A., Pourpak, Z., Naddafi, K., Nodehi, R.N., Alizadeh, Z., Rezaei, S., Faraji, M., 2019. An in vitro method to evaluate hemolysis of human red blood cells (RBCs) treated by airborne particulate matter (PM_{10}). MethodsX 6, 156–161. https://doi.org/10.1016/j.mex.2019.01.001

MEP (Ministry of Ecology and Environment of the People's Republic of China), 2012. National ambient air quality standards. http://www.mee.gov.cn/ywgz/fgbz/bz/bzwb/dqhjbh/dqhjzlbz/201203/t20120302_224165.htm. (Accessed 29 February 2012) (in Chinese).

MEP (Ministry of Ecology and Environment of the People's Republic of China), 2017. Action plan for comprehensive control of atmospheric pollution in autumn and winter of Beijing-Tianjin-Hebei region in 2017–2018. http://www.mee.gov.cn/gkml/hbb/ bwj/201708/t20170824_420330.htm.

(Accessed 21 August 2017) (in Chinese).

Niu, X.Y., Jones, T., Berube, K.A., Chuang, Hsiao-Chi, Sun, J., Ho, K.F., 2021. The oxidative capacity of indoor source combustion derived particulate matter and resulting respiratory toxicity. *Science of the Total Environment 767*, 144391. 10.1016/j.scitotenv.2020.144391

O'Shea, M.J., Vigliaturo, R., Choi, J.K., McKeon, T.P., Krekeler, M.P.S., Gieré, R., 2021. Alteration of yellow traffic paint in simulated environmental and biological fluids. *Science of the Total Environment 750*: 141202. 10.1016/j.scitotenv.2020.141202

Pan, Y.P., Wang, Y.S., Sun, Y., Tian, S.L., Cheng, M.T., 2013. Size-resolved aerosol trace elements at a rural mountainous site in Northern China: importance of regional transport. *Sci Total Environ 461-462*, 761-771. 10.1016/j.scitotenv.2013.04.065.

Pirozzi, C. S., Jones, B. E., VanDerslice, J. A., Zhang, Y., Paine, R., III, Dean, N. C. 2018. Short-term air pollution and incident pneumonia a case-crossover study. *Annals of the American Thoracic Society 15*, 449-459. 10.1513/AnnalsATS.201706-495OC.

Ren, Y., Luo, Q., Zhuo, S., Hu, Y., Shen, G., Cheng, H., Tao, S., 2021. Bioaccessibility and public health risk of heavy Metal(loid)s in the airborne particulate matter of four cities in northern China. *Chemosphere 277*, 130312. 10.1016/j.chemosphere.2021.130312.

Rohra, H., Tiwari, R., Khare, P., Taneja, A., 2018. Indoor-outdoor association of particulate matter and bounded elemental composition within coarse, quasi-accumulation and quasi-ultrafine ranges in residential areas of northern India. *Sci Total Environ 631-632*, 1383-1397. 10.1016/j.scitotenv.2018.03.095.

Shao, L.Y., Li, J., Zhang, M.Y., Wang, X.M., Li, Y.W., Jones, T.P., Feng, X.L., Silva, L.F.O., Li, W.J., 2021. Morphology, composition and mixing state of individual airborne particles: Effects of the 2017 Action Plan in Beijing, China. *Journal of Cleaner Production 329.* 10.1016/j.jclepro.2021.129748.

Shao, L.Y., Hou, C., Geng, C.M., Liu, J.X., Hu, Y., Wang, J., Jones, T.P., Zhao, C.M., BeruBe, K.A., 2016. The oxidative potential of PM_{10} from coal, briquettes and wood charcoal burnt in an experimental domestic stove. *Atmospheric Environment 127*, 372-381. 10.1016/j.atmosenv.2015.12.007.

Shao, L.Y., Hu, Y., Wang, J., Hou, C., Yang, Y.Y., Wu, M.Y., 2013. Particle-induced oxidative damage of indoor PM_{10} from coal burning homes in the lung cancer area of Xuan Wei, China. *Atmospheric Environment 77*, 959-967. 10.1016/j.atmosenv.2013.05.079.

Shao, L.Y., Li, J.J., Zhao, H.Y., Yang, S.S, Li, H., Li, W.J., Jones, T.P., Sexton, K., BéruBé, K.A., 2007. Associations between particle physicochemical characteristics and oxidative capacity: An indoor PM_{10} study in Beijing, China. *Atmospheric Environment 41*, 5316-5326. 10.1016/j.atmosenv.2007.02.038.

Shao, L.Y., Shi, Z.B., Jones, T.P., Li, J.J., Whittaker, A.G., BéruBé, K.A., 2006. Bioreactivity of particulate matter in Beijing air: results from plasmid DNA assay. *Science of the Total Environment 367*, 261-272.

10.1016/j.scitotenv.2005.10.009.

Shao, L.Y., Hu, Y., Shen, R.R., Schafer, K., Wang, J., Wang, J.Y., Schnelle-Kreis, J., Zimmermann, R., BeruBe, K.K., Suppan, P., 2017. Seasonal variation of particle-induced oxidative potential of airborne particulate matter in Beijing. *Sci Total Environ 579*, 1152-1160. 10.1016/j.scitotenv.2016.11.094.

Sheehan, M.C., Lam, J., Navas-Acien, A., Chang, H.H., 2016. Ambient air pollution epidemiology systematic review and meta-analysis: A review of reporting and methods practice. *Environment International 92-93*, 647-656. 10.1016/j.envint.2016.02.016.

Shen, R.R., Schaefer, K., Schnelle-Kreis, J., Shao, L.Y., Norra, S., Kramar, U., Michalke, B., Abbaszade, G., Streibel, T., Fricker, M., Chen, Y., Zimmermann, R., Emeis, S., Schmid, H.P., 2016. Characteristics and sources of PM in seasonal perspective - A case study from one year continuously sampling in Beijing. *Atmospheric Pollution Research 7*, 235-248. 10.1016/j.apr.2015.09.008.

Silva, L.F., Santosh, M., Schindler, M., Gasparotto, J., Dotto, G.L., Oliveira, M.L., Hochella Jr, M.F., 2021. Nanoparticles in fossil and mineral fuel sectors and their impact on environment and human health: A review and perspective. *Gondwana Research* 92, 184-201. 10.1016/j.gr.2020.12.026.

Song, C.B., He, J.J., Wu, L., Jin, T.S., Chen, X., Li, R.P., Ren, P.P., Zhang, L., Mao, H.Q., 2017. Health burden attributable to ambient $PM_{2.5}$ in China. *Environmental Pollution 223*, 575-586. 10.1016/j.envpol.2017.01.060.

Song, F., Gao, Y., 2011. Size distributions of trace elements associated with ambient particular matter in the affinity of a major highway in the New Jersey–New York metropolitan area. *Atmospheric Environment 45*, 6714-6723. 10.1016/j.atmosenv.2011.08.031.

Song, X.Y., Shao, L.Y., Yang, S.S., Song, R.Y., Sun, L.M., Cen, S.H., 2015. Trace elements pollution and toxicity of airborne PM_{10} in a coal industrial city. *Atmospheric Pollution Research 6*, 469-475. 10.5094/apr.2015.052.

Sun, Z.Q., Shao, L.Y., Mu, Y.J., Hu, Y., 2014. Oxidative capacities of size-segregated haze particles in a residential area of Beijing. *Journal of Environmental Sciences 26*, 167-174. 10.1016/S1001-0742(13)60394-0.

Tan, J.H., Duan, J.C., Zhen, N.J., He, K.B., Hao, J.M., 2016. Chemical characteristics and source of size-fractionated atmospheric particle in haze episode in Beijing. *Atmospheric Research 167*, 24-33. 10.1016/j.atmosres.2015.06.015.

The State Council of China, 2013. Air pollution prevention and control action plan. http:// www.gov.cn/zwgk/2013-09/12/content_2486773.htm. (Accessed 12 September 2013) (in Chinese).

Tian, Y., Li, Y., Liang, Y., Xue, Q., Feng, X., Feng, Y., 2021. Size distributions of source-specific risks of atmospheric heavy metals: An advanced method to quantify source contributions to size-segregated respiratory exposure. *Journal of Hazardous Materials 407*. 10.1016/j.jhazmat.2020.124355.

Wang, Y. J., Bao, S. W., Wang, S. X., Hu, Y. T., Shi, X., Wang, J. D., Zhao, B., Jiang, J. K., Zheng, M., Wu, M. H., Russell, A. G., Wang, Y. H., Hao, J. M., 2017. Local and regional contributions to fine particulate matter in Beijing during

heavy haze episodes. *Science of the Total Environment 580*, 283-296. 10.5194/acp-19-5791-2019

Wang, Y., Li, Y., Qiao, Z., Lua, Y., 2019. Inter-city air pollutant transport in the Beijing-Tianjin-Hebei urban agglomeration: Comparison between the winters of 2012 and 2016. *Journal of Environmental Management 250*, 109520. 10.1016/j.jenvman.2019.109520.

Wang, Y.C., Wang, Q.Y., Ye, J.H., Li, L., Zhou, J., Ran, W.K, Zhang, R.J., Wu, Y.F., Cao, J.J., 2020. Chemical composition and sources of submicron aerosols in winter at a regional site in Beijing-Tianjin-Hebei region: Implications for the Joint Action Plan. *Science of the Total Environment 719*, 137547. 10.1016/j.scitotenv.2020.137547.

Wu, Y.H., Yang, X., Wang, H.N., Jia, G., Wang, T.C., 2021. Relationship between ambient $PM_{2.5}$ exposure and blood cadmium level in children under 14 years in Beijing, China. *Journal of Hazardous Materials 403*, 123871. 10.1016/j.jhazmat.2020.123871.

Xiao, Z.H., Shao, L.Y., Zhang, N., Wang, J., Chuang, H.-C., Deng, Z.Z., Wang, Z., BéruBé, K.A., 2014. A toxicological study of inhalable particulates in an industrial region of Lanzhou City, northwestern China: Results from plasmid scission assay. *Aeolian Research 14,* 25-34. 10.1016/j.aeolia.2014.03.004.

Xing, J.P., Shao, L.Y., Zhang, W.B., Peng, J.F., Wang, W.H., Shuai, S.J., Hu, M., Zhang, D.Z., 2020. Morphology and size of the particles emitted from a gasoline-direct-injection-engine vehicle and their ageing in an environmental chamber. *Atmospheric Chemistry and Physics 20*, 2781-2794. 10.5194/acp-20-2781-2020.

Xu, X., Zhang, T., 2020. Spatial-temporal variability of $PM_{2.5}$ air quality in Beijing, China during 2013-2018. *Journal of Environmental Management 262*.110263. 10.1016/j.jenvman.2020.110263.

Xu, X.H., Ha, S.D., Kan, H.D., Hu, H., Curbow, B.A., Lissaker, C.T.K., 2013. Health effects of air pollution on length of respiratory cancer survival. *BMC Public Health 13*, Artn 800 10.1186/1471-2458-13-800.

Xue, T., Liu, J., Zhang, Q., Geng, G.N., Zheng, Y.X., Tong, D., Liu, Z., Guan, D.B., Bo, Y., Zhu, T., He, K.B., Hao, J.M., 2019. Rapid improvement of $PM_{2.5}$ pollution and associated health benefits in China during 2013–2017. *Science China Earth Sciences 62*, 1847-1856. 10.1007/s11430-018-9348-2.

Zhang, Q., Zheng, Y., Tong, D., Shao, M., Wang, S., Zhang, Y., Xu, X., Wang, J., He, H., Liu, W., Ding, Y., Lei, Y., Li, J., Wang, Z., Zhang, X., Wang, Y., Cheng, J., Liu, Y., Shi, Q., Yan, L., Geng, G., Hong, C., Li, M., Liu, F., Zheng, B., Cao, J., Ding, A., Gao, J., Fu, Q., Huo, J., Liu, B., Liu, Z., Yang, F., He, K., Hao, J. 2019. Drivers of improved $PM_{2.5}$ air quality in China from 2013 to 2017. *Proceedings of the National Academy of Sciences 116*, 24463-24469. 10.1073/pnas.1907956116.

Zhang, M.Y., Shao, L.Y., Jones, T.P., Hu, Y., Adams, R.J., BéruBé, K., 2021. Hemolysis of PM_{10} on RBCs in vitro: An indoor air study in a coal-burning lung cancer epidemic area. *Geoscience Frontiers*. 10.1016/j.gsf.2021.10117610.1016/j.gsf. 2021.101176.

Zheng, G.J., Duan, F.K., Su, H., Ma, Y.L., Cheng, Y., Zheng, B., Zhang, Q., Huang, T., Kimoto, T., Chang, D., Poschl, U., Cheng, Y.F., He, K.B., 2015a. Exploring the severe winter haze in Beijing: the impact of synoptic weather, regional transport and heterogeneous reactions. *Atmospheric Chemistry and Physics 15*, 2969-2983. 10.5194/acp-15-2969-2015.

Zheng, S., Pozzer, A., Cao, C.X., Lelieveld, J., 2015b. Long-term (2001-2012) concentrations of fine particulate matter ($PM_{2.5}$) and the impact on human health in Beijing, China. *Atmospheric Chemistry and Physics 15*, 5715-5725. 10.5194/acp-15-5715-2015.

Zhou, W., Chen, C., Lei, L., Fu, P.Q., Sun, Y.L., 2021. Temporal variations and spatial distributions of gaseous and particulate air pollutants and their health risks during 2015-2019 in China. *Environmental pollution 272*, 116031. 10.1016/j.envpol.2020.116031.

Figures and Tables

Tables:

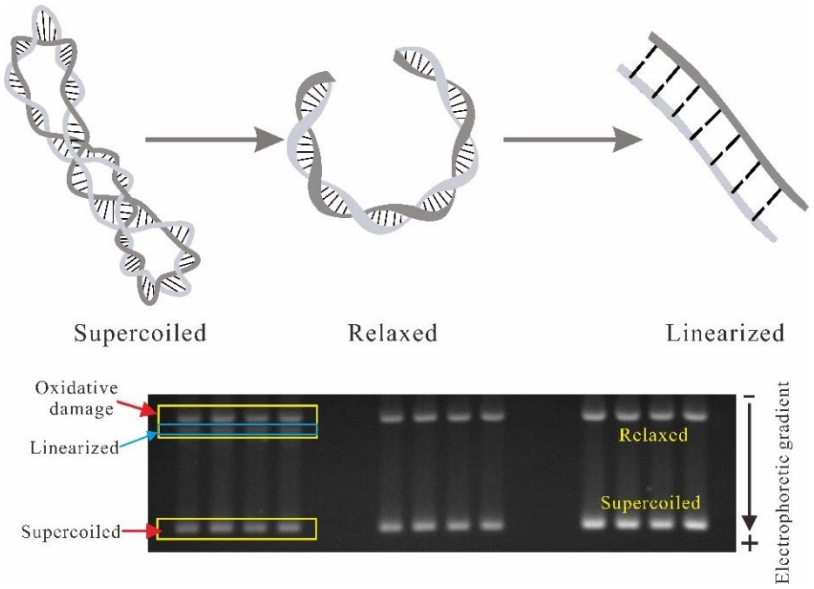

Fig.1 Schematic illustration showing the principle of the plasmid scission assay.

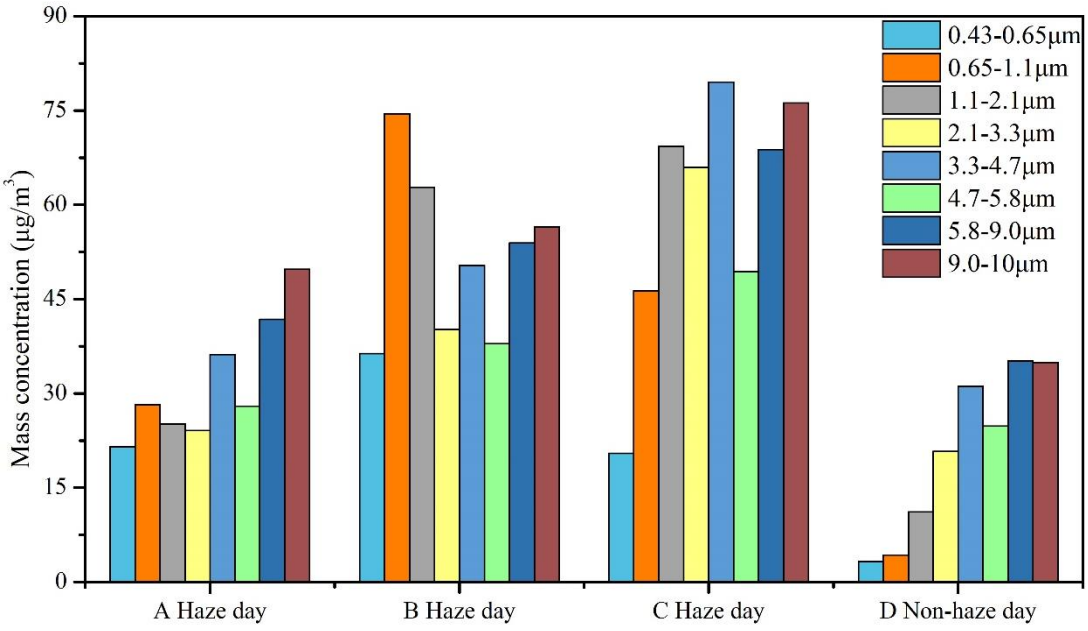

Fig.2 Mass concentrations of size-segregated particulate matter in the size range from 0.43 μm to 10 μm

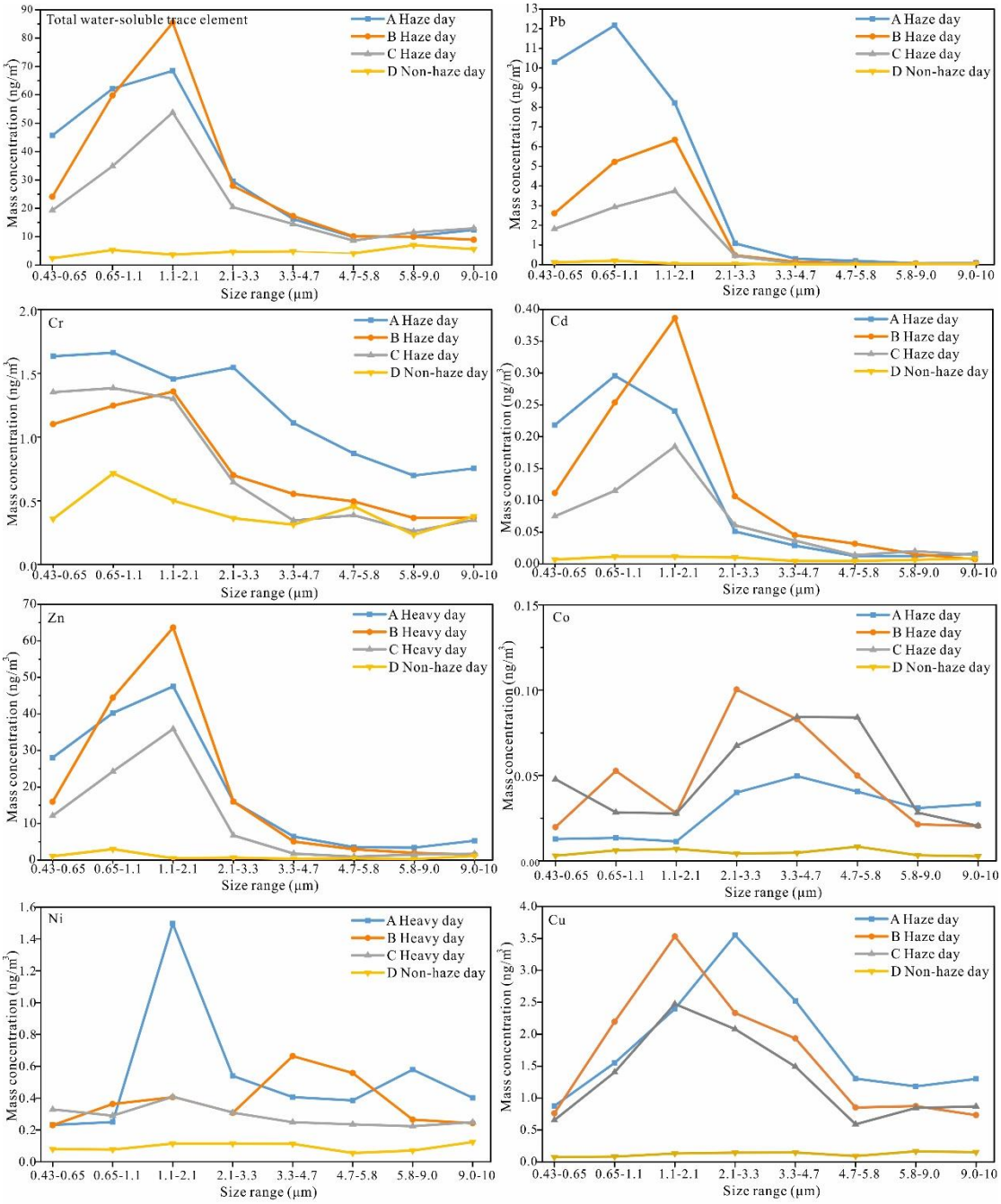

Fig.3 Mass-size distribution of total WSTE and individual water-soluble Pb, Cr, Cd, Zn, Co, Ni, and Cu over the particle size range with different particle sizes in haze and non-haze days

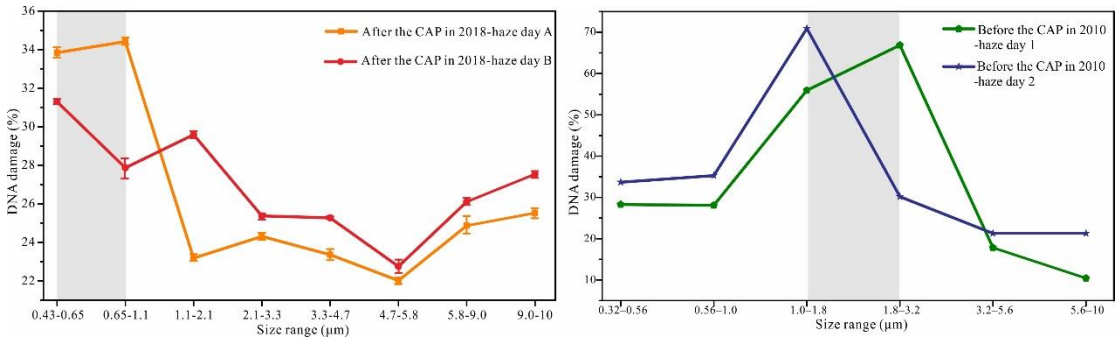

Fig.4 The particle-induced DNA damage at the particle dosage of 100 μg/ml over the particle size range in haze days before and after the CAP. The data in 2010 is from Sun et al. (2014). The grey shadow areas represent the maximum of DNA damage in different particle size ranges in haze days.

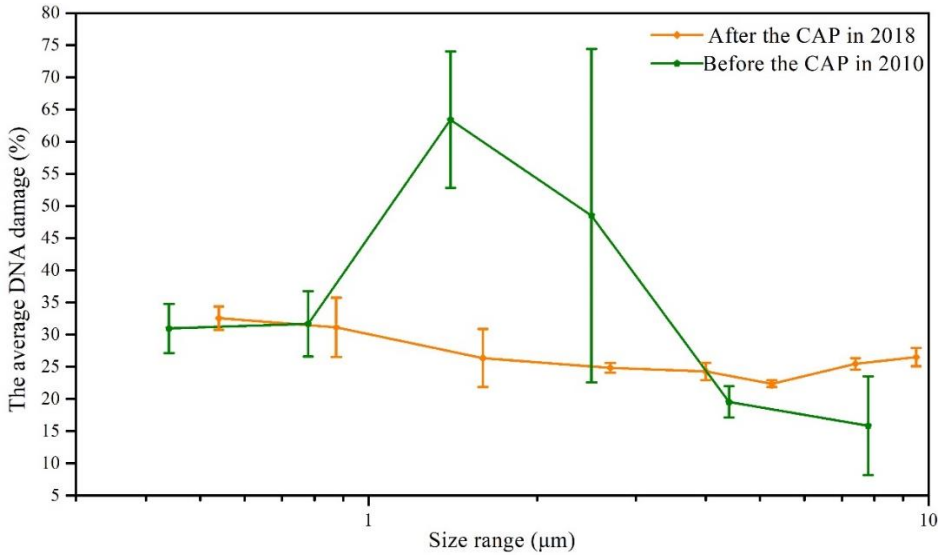

Fig.5 The average DNA damage induced by size-segregated particles at the particle dosage of 100 μg/ml in haze days before and after the CAP. The data in 2010 is from Sun et al. (2014).

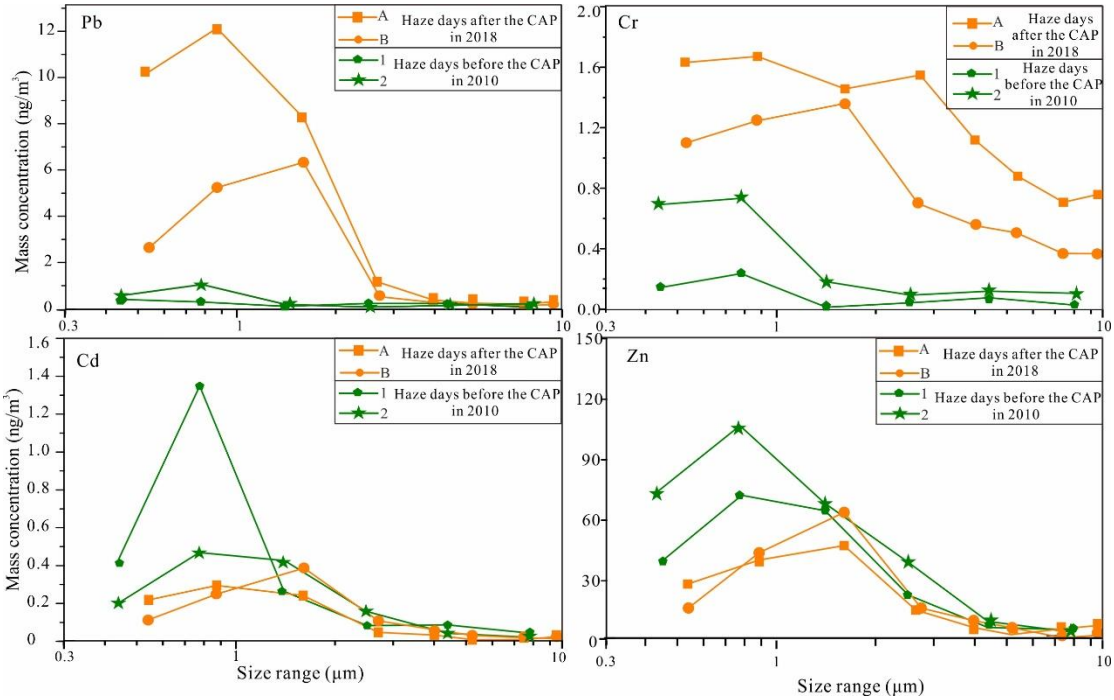

Fig.6 A comparison of the mass concentration of WSHM before and after the CAP. The data in 2010 is from Sun et al. (2014).

Table 1 Plasmid DNA damage rate (%) induced by size-segregated airborne particles at the particle dosage of 100 μg/ml for samples

Size range (μm)	A Haze day	B Haze day	C Haze day	D Non-haze day	Blank
0.43-0.65	33.84	31.29	31.58	—	< 10
0.65-1.1	34.42	27.87	30.17	—	
1.1-2.1	23.18	29.58	25.10	16.94	
2.1-3.3	24.31	25.37	22.85	17.45	
3.3-4.7	23.36	25.27	26.13	19.34	
4.7-5.8	22.02	22.75	25.21	18.32	
5.8-9.0	24.87	26.10	23.60	13.68	
9.0-10	25.53	27.54	26.27	18.56	

Table 2 The Pearson correlation between the concentrations of WSHM (μg/g) and DNA damage rate at 100 μg/mL for the size-segregated particles

The type of elements	total	Pb	Cr	Cd	Zn	Cu	Co	Ni
Correlation coefficient	0.558[a]	0.595[a]	0.593[a]	0.590[a]	0.533[a]	0.316	0.303	0.114

[a] Significantly correlated at the 0.01 level (both sides).

Supplementary material

Fig.S1 The hourly variation of $PM_{2.5}$ mass concentration during the pollution period

Table S1 Meteorological condition during the sampling periods

Table S2 Contents of 7 typical WSHM in size-segregated particles during the sampling periods

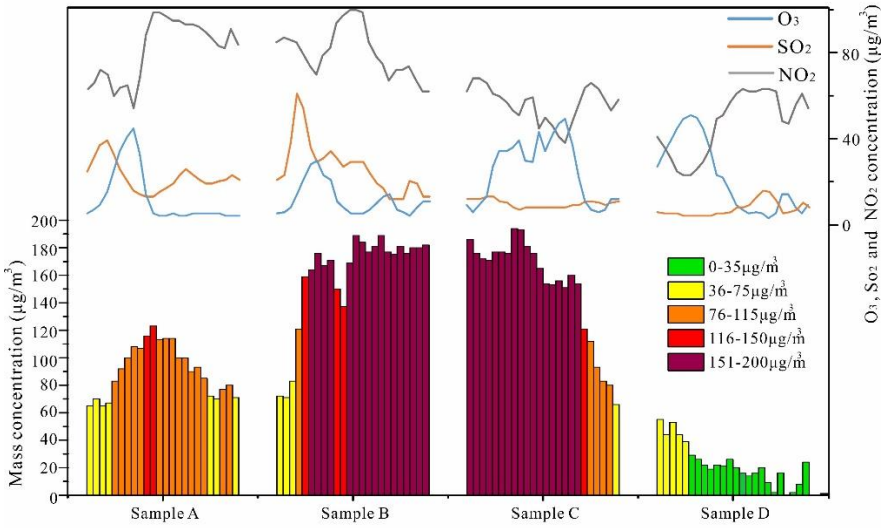

Fig.S1 The hourly variation of $PM_{2.5}$, NO_2, SO_2, O_3 mass concentration during the pollution period

Table S1 Meteorological condition during the sampling periods

Time period	No.	Temperature(℃)			Relative humidity(%)			Pressure(hPa)		
		Mini.	Max.	Ave.	Mini.	Max.	Ave.	Mini.	Max.	Ave.
2018.11.30-2018.12.01	A	3.7	9.1	7.9	43.5	51.2	46.8	1018.7	1019.4	1018.9
2018.12.01-2018.12.02	B	5.2	5.8	5.4	47.7	95.9	52.6	1009.7	1020.2	1018.6
2018.12.02-2018.12.03	C	5.3	7	5.9	13.9	100	44.9	1010.9	1016.2	1014.3
2018.12.03-2018.12.04	D	3.2	5.7	4.5	13.4	14.9	14	1017.1	1023.4	1019.9

According to the analysis of monitoring data and meteorological data, C was seriously influenced by wind-blown mineral dust.

Table S2 Contents of 7 typical WSHM in size-segregated particles during the sampling periods (Unit: ppt)

Size range (μm) / Trace elements	0.43-0.56	0.56-1.1	1.1-2.1	2.1-3.3	3.3-4.7	4.7-5.8	5.8-9	9-10	0.43-0.56	0.56-1.1

Cr	15541	22352	16673	18828	17115	11879	8616	7266	13252	11244
Co	316	416	466	605	618	155	166	123	246	193
Ni	2202	3346	17165	6577	6259	5257	7148	3873	2762	3277
Cu	8333	20840	27506	43265	38910	17783	14616	12532	9165	19815
Zn	266517	541056	545199	194726	99197	47873	42060	51197	191974	401097
Cd	2077	3977	2758	623	445	170	151	156	1344	2290
Pb	97877	163697	94267	13089	4638	2596	791	887	31335	47172

Size range (μm) / Trace element	1.1-2.1	2.1-3.3	3.3-4.7	4.7-5.8	5.8-9	9-10	0.43-0.56	0.56-1.1	1.1-2.1	2.1-3.3	3.3-4.7	4.7-5.8
Cr	15517	9136	6310	7055	5242	4931	13782	14746	12972	6895	3664	3763
Co	571	1083	1145	399	756	265	208	300	838	900	716	270
Ni	4634	3999	7567	7945	3796	3238	3350	3081	4065	3288	2631	2287
Cu	40374	30453	22044	12140	12541	9798	6675	14953	24681	22217	15840	5743
Zn	727730	208432	57446	42204	28069	20698	123609	258221	357903	72140	18664	9277
Cd	4418	1387	516	453	220	100	766	1225	1843	651	390	135

Pb	72557	6165	1698	833	730	733	18480	31153	37387	4756	638	503

Size range (μm) / Trace element	5.8-9	9-10	0.43-0.56	0.56-1.1	1.1-2.1	2.1-3.3	3.3-4.7	4.7-5.8	5.8-9	9-10
Cr	2635	3067	12843	14892	6819	3619	3616	5293	2270	3718
Co	286	419	97	67	113	47	50	81	60	30
Ni	2247	2174	2822	1584	1547	1133	1295	631	677	1213
Cu	8511	7619	2635	1731	1806	1458	1718	1066	1624	1491
Zn	15082	15172	38589	62049	6377	6124	3554	5293	2159	11260
Cd	202	126	247	242	160	102	55	55	63	83
Pb	237	470	3973	4072	620	456	80	100	267	282